Biochimica et Biophysica Acta 1848 (2015) 712–720

Contents lists available at ScienceDirect

Biochimica et Biophysica Acta

journal homepage: www.elsevier.com/locate/bbamem

Influence of the lipid membrane environment on structure and activity of the outer membrane protein Ail from *Yersinia pestis*

Yi Ding [a], L. Miya Fujimoto [a], Yong Yao [a], Gregory V. Plano [b], Francesca M. Marassi [a,*]

[a] Sanford-Burnham Medical Research Institute, La Jolla, CA 92037, USA
[b] University of Miami Miller School of Medicine, Miami, FL 33101, USA

ARTICLE INFO

Article history:
Received 7 July 2014
Received in revised form 24 October 2014
Accepted 19 November 2014
Available online 27 November 2014

Keywords:
Ail
Nanodisc
NMR
Membrane protein
Structure
Activity

ABSTRACT

The surrounding environment has significant consequences for the structural and functional properties of membrane proteins. While native structure and function can be reconstituted in lipid bilayer membranes, the detergents used for protein solubilization are not always compatible with biological activity and, hence, not always appropriate for direct detection of ligand binding by NMR spectroscopy. Here we describe how the sample environment affects the activity of the outer membrane protein Ail (attachment invasion locus) from *Yersinia pestis*. Although Ail adopts the correct β-barrel fold in micelles, the high detergent concentrations required for NMR structural studies are not compatible with the ligand binding functionality of the protein. We also describe preparations of Ail embedded in phospholipid bilayer nanodiscs, optimized for NMR studies and ligand binding activity assays. Ail in nanodiscs is capable of binding its human ligand fibronectin and also yields high quality NMR spectra that reflect the proper fold. Binding activity assays, developed to be performed directly with the NMR samples, show that ligand binding involves the extracellular loops of Ail. The data show that even when detergent micelles support the protein fold, detergents can interfere with activity in subtle ways.

1. Introduction

The biological functions and molecular structures of proteins are highly dependent on the physical and chemical properties of the surrounding environment [1]. Just as water is essential for supporting the native states of soluble proteins, the lipid bilayer is critical for preserving the functional and structural integrity of membrane proteins. By contrast, the detergents used to solubilize membrane proteins for structural studies by NMR and crystallography can interfere with biological activity in multiple ways [2].

Among the methods for three-dimensional molecular structure determination, the principal advantage of NMR spectroscopy is its ability to examine proteins in samples that are very close to their native environments. This enables structure and biological function to be characterized in the same sample and useful structure–activity correlations to be established by direct spectroscopic detection of ligand binding or conformational changes [3]. Various NMR experimental approaches and sample types have been developed for membrane protein structural studies in detergent-free lipid samples. Solid-state NMR methods can be used for proteins in a variety of lipid bilayer assemblies, including planar supported lipid bilayers, lipid bilayer macrodiscs and liposomes [4–10]. More recently, lipid bilayer nanodiscs [11,12] have been used effectively for solution NMR studies of membrane proteins [13–24].

Here we describe the influence of the sample environment on the activity of the outer membrane protein Ail (attachment invasion locus) from *Yersinia pestis*, an extremely pathogenic organism with a long history of precipitating massive human pandemics [25–27]. We show that Ail in detergent micelles adopts an eight-stranded β-barrel conformation, with three intracellular loops (IL1–3) and four extracellular loops (EL1–4), similar to that of its crystal structure [28]. However, we find that the micellar detergent concentrations required for high resolution NMR spectroscopy are not compatible with functional assays of ligand binding. By contrast, optimized preparations of Ail in phospholipid bilayer nanodiscs support both function and structure, and can be used for parallel activity and NMR studies on exactly the same samples.

The pathogenicity of *Y. pestis* is associated with its exceptional abilities to proliferate in diverse environments and overcome the defenses of the human host. *Y. pestis* Ail is an essential factor contributing to these properties by mediating cell adhesion [29,30], promoting bacterial cell auto-aggregation [29] and conferring serum resistance [29,31]. Ail-mediated cell adhesion is essential for delivering the *Yersinia* outer protein (Yop) effectors that protect the bacterial cell from phagocytosis and

Abbreviations: DDM, n-dodecyl-β-D-maltopyranoside; DePC, n-decyl-phosphocholine; DHPC, 1,2-dihexyl-sn-glycero-3-phosphocholine; DMPC, 1,2-dimyristoyl-sn-glycero-3-phosphatidylcholine; DMPG, 1,2-dimyristoyl-sn-glycero-3-phosphatidylglycerol; DPC, n-dodecyl-phosphocholine; ELISA, enzyme linked immunosorbent assay; IPTG, isopropyl 1-thio-β-D-galactopyranoside; LDAO, n-dodecyl-N,N-dimethylamine-N-oxide; LPPG, 16,0-lysophosphatidylglycerol; MSP, membrane scaffold protein; PAGE, polyacrylamide gel electrophoresis; SDS, sodium dodecylsulfate

* Corresponding author at: Sanford-Burnham Medical Research Institute, 10901 North Torrey Pines Road, La Jolla, CA 92037, USA. Tel.: +1 858 795 5282; fax: +1 858 713 6268.
E-mail address: fmarassi@sbmri.org (F.M. Marassi).

http://dx.doi.org/10.1016/j.bbamem.2014.11.021
0005-2736/

interfere with the host's inflammatory response, enabling *Y. pestis* to survive and multiply extracellularly [30,32]. The interactions of *Y. pestis* Ail with the extracellular matrix proteins fibronectin and laminin have been shown to be important for both cell adhesion and Yop delivery [28,33,34], and amino acid residues in Ail's extracellular loops have been shown to play important roles in the adhesion of *Y. enterocolitica* and *Y. pestis* [35,36] as well as in the invasion and serum resistance of *Y. enterocolitica* [35]. The ability to perform parallel NMR and functional activity assays on samples of Ail in lipid bilayers, free of interference from detergent molecules, paves the way for structure–activity NMR studies and the development of Ail-targeted molecular intervention.

2. Materials and methods

2.1. Expression and purification of Ail

Wild-type Ail and C-terminal His-tagged Ail (Ail–His) were prepared by cloning the gene corresponding to mature *ail* from *Y. pestis* KIM 10 (gene *y1324* without signal sequence) in the *Escherichia coli* pET-30b plasmid vector (EMD). For wild-type Ail, the gene was cloned between the *Nde*I and *Xho*I restriction sites of the plasmid. For His-tagged Ail, the gene was cloned between *Nde*I and *Kpn*I sites, to express Ail plus the His tag encoded after the *Kpn*I site of pET-30b. The expressed amino acid sequences of Ail and Ail–His begin with an extra N-terminal methionine before residue Glu1 of the native sequence (Fig. S1). The sequence of Ail terminates with the native residue Phe156, while Ail–His includes 33 additional C-terminal residues from the His tag of the pET-30b vector. The longer linker sequence preceding the His tag was essential for folding Ail–His. Protein folding was abolished when short His tags were directly appended to the C-terminus of Ail.

The *ail*-encoded plasmids were transformed in *E. coli* BL21 (DE3) cells and positive clones were grown at 37 °C, in minimal M9 medium [37], supplemented with 1 mM thiamine, and 35 μg/mL kanamycin to maintain plasmid selectivity. Cells were grown to a cell density of $OD_{600} = 0.6$, before induction with 1 mM IPTG (isopropyl 1-thio-β-D-galactopyranoside) for 3 h, then harvested by centrifugation (7200 ×g, 4 °C, 15 min), and stored at −80 °C overnight. For ^{15}N, ^{13}C and ^{2}H labeling of Ail, bacteria were grown in M9 medium prepared in 99% D_2O and containing 1 g/L of U-99%$^{15}NH_4Cl$ plus 2 g/L of U-99%^{13}C-glucose as the sole sources of N and C. All isotopes were from Cambridge Isotope Laboratories. Bacteria were adapted to culture in $^{2}H_2O$ by adding 1 mL of $^{2}H_2O$ M9 media to a 1 mL H_2O M9 starter culture every 2 h, until the volume reached 5 mL, and then growing overnight. After transferring this overnight culture into 20 mL of fresh $^{2}H_2O$ M9 media, growth was continued for 4 h at 37 °C to a cell density of $OD_{600} = 1.0$, then the entire volume was placed into 475 mL of fresh $^{2}H_2O$ M9 and cell growth and induction were carried out as described above.

Cells from 1 L of culture were suspended in 30 mL of buffer A (20 mM Tris–Cl, pH 8.0) and lysed by two passes through a French Press. After removing the soluble cell fraction by centrifugation (48,000 ×g, 4 °C, 30 min) the insoluble pellet, enriched in inclusion bodies, was suspended in 30 mL of buffer A, supplemented with 2% Triton-X, for 1 h, at 37 °C. The soluble fraction was removed by a second centrifugation step (48,000 ×g, 4 °C, 30 min) and the remaining pellet was first washed by suspension and centrifugation in 30 mL of water to remove residual detergent, and then dissolved in 30 mL of buffer B (20 mM Na-acetate, pH 5.0, 8 M urea) for Ail, or buffer A for Ail–His. Any insoluble material remaining after incubation at 37 °C for 1 h, was removed by centrifugation (48,000 ×g, 4 °C, 30 min). Ail and Ail–His were purified by cation exchange chromatography (HiTrap SP/HP 5 mL column, GE Healthcare) in buffer B with a NaCl gradient (Ail), or Ni affinity chromatography (HisTrap FF 5 mL column, GE Healthcare) in buffer A plus 8 M urea and 500 mM NaCl (Ail–His). Both Ail and Ail–His were further purified by size exclusion chromatography (Sephacryl S-200 HR HiPrep 16/60 column, GE Healthcare) in buffer B supplemented with 150 mM NaCl. Purified Ail was precipitated by dialysis (10 kDa molecular weight cutoff) against water, lyophilized, and stored at −20 °C.

2.2. Expression and purification of membrane scaffold protein

Two variants of membrane scaffold protein (MSP) were expressed and purified as described previously: MSP1D1 [12] and MSP1D1Δh5 [18] lacking the fifth helical segment of MSP1D1. The C-terminal His tags were removed by proteolysis with tobacco etch virus and the MSPs purified by Ni-affinity chromatography. The pET-28a-MSP1D1 plasmid developed by Sligar and coworkers [38] was obtained from Addgene (Addgene plasmid 20061). A nucleotide encoding MSP1D1Δh5 was obtained from GenScript and cloned into the NcoI and HindIII restriction sites of pET-28a (EMD) by restriction and digestion with Gibson Assembly Master Mix (New England Biolabs).

2.3. SDS PAGE and Western blot analysis

Proteins were analyzed by 4–12% Bis–Tris SDS (sodium dodecyl sulfate) polyacrylamide gel electrophoresis (PAGE) and visualized by staining with Coomassie brilliant blue, or transferred to nitrocellulose for Western immuno-blotting and visualized using antibody-conjugated alkaline phosphatase (Biorad) with 5-bromo-4-chloro-3′-indolyphosphate p-toluidine salt substrate and nitro-blue tetrazolium chloride developer. Western dot blots were performed on nitrocellulose in a similar manner, without prior separation on SDS-PAGE. Ail–His was probed with mouse anti-His monoclonal antibody (Qiagen; 1/5000 dilution). MSP was probed with goat anti-ApoA1 polyclonal antibody (Millipore; 1/1000 dilution). Ail was probed with rabbit anti-Ail-EL2 antibody (1/1000 dilution) specific for the second extracellular loop (EL2) of Ail. Anti-Ail-EL2 antibody was raised in rabbits against Keyhole limpet hemocyanin (KLH)-peptide (NH_2-CTRRGFEESVDGFKLIDGDF-COOH) conjugates, and purified via peptide affinity chromatography (Proteintech, Chicago, IL).

2.4. Protein refolding in detergent

Purified, lyophilized protein (1 mg of Ail or Ail–His) was dissolved in 100 μL of 6 M urea and added dropwise to 600 μL of refolding buffer (20 mM glycine, pH 10.2, 5 mM EDTA, 600 mM arginine, 300 mM KCl) containing 47 mM n-decyl-phosphocholine (DePC; Anatrace). The solution was gently stirred overnight at room temperature to achieve complete refolding, and then concentrated to 50 μL using a Vivaspin 500 centrifugal concentrator with 10 kDa cutoff (VivaProducts). The buffer was exchanged by consecutive addition of 150 μL of buffer C (5 mM Na-PO_4, pH 6.8, 5 mM NaCl, 19 mM DePC) and concentration to 50 μL, repeated four times to obtain a solution containing 1 mM Ail and 130–180 mM DePC.

The protein concentration was determined by measuring the UV absorbance at 280 nm, with a molar extinction coefficient of 28,880 M^{-1} cm^{-1}, whose value was confirmed by an independent Bradford assay. The DePC concentration was estimated by monitoring the intensity of the ^{1}H NMR peak from the trimethylamino protons at 3.15 ppm.

Protein folding was assessed by monitoring the shift in SDS-PAGE apparent molecular weight that correlates with the transition from unfolded to folded states of transmembrane β-barrels [39], and by solution NMR spectroscopy, where folded Ail yields high quality $^{1}H/^{15}N$ correlation spectra with ^{1}H chemical shifts dispersed over more than 3 ppm, and unfolded Ail yields spectra with all ^{1}H resonances collapsed within 0.5 ppm [40], as expected for random coil.

2.5. Protein reconstitution in phospholipid nanodiscs

Refolded Ail was assembled into nanodiscs following published protocols [12,38]. Briefly, MSP1D1Δh5 (MSP) was added to a 3/1 M mixture of dimyristoyl-phosphatidyl-choline (DMPC, 5.8 mg) and dimyristoyl-phosphatidyl-glycerol (DMPG, 2 mg), dissolved in 500 μL of nanodisc buffer (20 mM Tris–Cl, pH 7.5, 100 mM NaCl, 1 mM EDTA) containing Na-cholate at a lipid/cholate molar ratio of 1/2. The mixture was incubated at room temperature for 30 min before adding refolded Ail (1–2 mg of Ail or Ail–His in 50 μL of 130–180 mM DePC) and nanodisc buffer to obtain 50–100 μM Ail in a volume of 1.14 mL. After incubation at room temperature for 1 h, 0.5 g of Biobeads SM-2 (Biorad; prewashed in nanodisc buffer) per mL of nanodisc preparation was added, and the mixture was further incubated at room temperature, with gentle shaking, for 3 h. Biobeads were removed by centrifugation and the resulting nanodiscs were washed twice with one sample volume of nanodisc buffer. The nanodisc solution was concentrated using a Vivaspin 500 concentrator with 30 kDa cutoff, to obtain 50 μL of 20 mg/mL (1.1 mM) Ail in nanodiscs. Detergent removal was assessed by ^{1}H NMR spectroscopy.

The optimal MSP/lipid ratio for Ail-containing nanodiscs was determined by screening with size exclusion chromatography (Superdex 75 10/300 GL column, GE Healthcare), performed in nanodisc buffer and monitored by detecting the UV absorbance at 280 nm of Ail and MSP. For solution NMR experiments, the nanodisc buffer was exchanged with NMR buffer containing 1 mM EDTA and 10% D_2O. The final concentration of Ail was 0.4 mM.

2.6. Protein reconstitution in phospholipid liposomes

Small unilamellar vesicles, were prepared by sonicating 20 mg of DMPC in 5 mL of Tris buffer saline (TBS; 50 mM Tris–Cl, pH 7.5, 150 mM NaCl). Refolded Ail (2 mg of Ail or Ail–His in 100 μL of 130–180 mM DePC) was added dropwise, at 37 °C, to the vesicles. The final DePC concentration was maintained at 50 mM by supplementing the mixture with DePC. After overnight incubation at 37 °C, the detergent was removed by dialysis (10 kDa cutoff) against four 1 L changes of TBS containing 1 g of Biobeads SM-2. Complete removal of detergent was assessed by ^{1}H NMR spectroscopy.

2.7. NMR experiments

For solution NMR, 216 μL of refolded Ail solution was diluted to 450 μL with NMR buffer (20 mM Na-PO_4, pH 6.8, 5 mM NaCl) containing 170 mM DePC and 10% $^{2}H_2O$. The final concentrations of Ail and DePC were 0.4–0.5 mM and 170 mM.

NMR experiments were performed at 45 °C on a Bruker AVANCE 600 MHz spectrometer equipped with a $^{1}H/^{15}N/^{13}C$ triple-resonance cryoprobe. $^{1}H/^{15}N$ TROSY-HSQC NMR spectra were obtained with 16 transients for $^{2}H/^{15}N$ labeled Ail in nanodiscs, or 8 transients for $^{2}H/^{15}N$ labeled Ail in DePC, for each of 256 *t1* points. Three-dimensional TROSY-based experiments [41,42] were used for $^{2}H/^{13}C/^{15}N$ labeled Ail in micelles or nanodiscs. Backbone resonance assignments for Ail in 170 mM DePC were obtained using HNCA [43], HNCACB [44] and ^{15}N-edited NOESY-HSQC (150 ms mixing time) experiments [45]. Heteronuclear $^{1}H/^{15}N$ NOE measurements [46] were made by performing difference experiments with and without 5 s saturation of the ^{1}H resonances between scans. $^{1}H/^{2}H$ exchange measurements for Ail in DePC micelles were made by calculating the ratios of intensities of the peaks from $^{1}H/^{15}N$ correlation NMR spectra in H_2O and $^{2}H_2O$. The NMR data were processed using NMRPipe [47] and analyzed using NMRView [48]. Chemical shifts were referenced to the H_2O resonance set to its expected position at 45 °C [49] and analyzed with TALOS+ [50].

2.8. Pull-down assays of protein activity

Pull-down assays were performed with Ni-NTA beads using non-His-tagged Ail and human plasma fibronectin (Sigma; F2006). Since we found that fibronectin spontaneously binds Ni-NTA, we used fibronectin-coated Ni-NTA beads as bait to pull-down Ail.

Non-His-tagged Ail (3 μL of 1 μg/μL solution in DePC or nanodiscs), fibronectin (10 μL of 1 μg/μL solution, Sigma F2006), or Ail plus fibronectin, were mixed in a total volume of 15 μL TBS and incubated overnight at 37 °C. For assays with Ail in detergents, the buffer was supplemented with the appropriate concentration of detergent. Ni-NTA agarose beads (30 μL, Millipore) were transferred to a Micro-Spin column (Pierce) and washed with two 100 μL volumes of TBS by suspension and centrifugation in a microfuge (2400 ×*g*, 1 min). The protein mixture was added to the washed Ni-NTA beads and the supernatant obtained by centrifugation was again loaded onto the Ni-NTA. This step was repeated three times to ensure complete binding of proteins with Ni-NTA affinity. After a third centrifugation step the supernatant was removed and the beads were washed by consecutive suspension in TBS and centrifugation. Three wash steps were performed, each with 15, 100 and 15 μL of TBS. The beads were finally eluted by three steps of suspension in 15 μL of SDS PAGE sample buffer (Life Technologies) followed by centrifugation. The supernatant fractions resulting from the loading, wash and elution steps were treated with 1 μL of 1 M dithiothreitol and analyzed by SDS PAGE.

Ail binding to heparin was assayed by mixing Ail (3 μL of 1 μg/μL solution in 4 mM DePC) with heparin-coated resin (Sigma) equilibrated in TBS in a Micro-Spin column. The beads were washed with two column volumes of TBS supplemented with 4 mM DePC and eluted with SDS sample buffer as described above.

2.9. Enzyme linked immunosorbent assays

Enzyme linked immunosorbent assays (ELISAs) were performed with antibody-conjugated horseradish peroxidase and its substrate o-Phenylenediamine (OPD; Pierce) added at a concentration of 0.5 mg/mL in stable peroxide substrate buffer (Thermo Scientific) to develop absorbance at 490 nm. Human plasma fibronectin (Sigma; F2006) was coated on 96-well plates (Nunc) at a concentration of 5 μg/mL in phosphate buffer saline (PBS). After coating overnight at 4 °C, the wells were washed three times with PBS, then blocked with TBS-milk (TBS with 3% milk) for 2 h at room temperature, and finally washed with TBST (TBS with 0.05% Tween-20 included to prevent non-specific binding). Incremental concentrations of Ail–His in TBST were added to the coated wells and the plates were incubated at 37 °C for 3 h and then at 4 °C overnight. Bound Ail–His was probed by adding mouse anti-His monoclonal antibody (Qiagen; 1:100 dilution in TBST-milk) to the wells and incubating for 2 h at room temperature. Unbound primary antibody and Ail were removed by washing three times with TBST-milk. Then, secondary goat anti-mouse antibody conjugated to horseradish peroxidase (Sigma; 1:10,000 dilution) was added, the plates were incubated for 1 h at room temperature, and finally washed three times with PBS and once with TBS, before adding fresh OPD to develop absorbance at 490 nm. Control experiments were performed by incubating the fibronectin-coated wells with the unrelated His-tagged protein ArfA-c from *Mycobacterium tuberculosis* and probing with the same anti-His primary antibody, or adding empty nanodiscs lacking Ail and probing for nanodisc MSP with rabbit anti-ApoA1 polyclonal antibody (Millipore; 1/800 dilution).

To assay the accessibility of Ail's EL2, Ail-containing nanodiscs were coated on 96-well plates (Nunc) at concentrations ranging from 2 to 0.03 μg/mL in PBS. After washing and blocking the wells as described above, Ail nanodiscs were probed using primary rabbit anti-Ail-EL2 antibody (1/1000 dilution in TBST-milk), followed by secondary goat anti-rabbit antibody conjugated to horseradish peroxidase (Sigma; 1:10,000 dilution), and substrate development, as described above.

3. Results and discussion

3.1. Ail is homogeneously refolded in detergent, liposomes and nanodiscs

Homogenous preparations of fully refolded *Y. pestis* Ail are obtained in DMPC liposomes, DMPC/DMPG nanodiscs as well as DePC and various other detergents (Fig. 1A, Fig. S2A [40]). A previous report showed that nanodiscs prepared with the shorter scaffold protein, MSP1D1Δh5, yield higher quality NMR spectra of the outer membrane protein OmpX than those prepared with MSP1D1 [18]. Our initial experiments indicated that the same is true for Ail (Fig. S3), therefore, we used MSP1D1Δh5 (henceforth referred to as MSP) for all subsequent sample optimizations and studies. The presence of DMPG helps prevent sample aggregation and provides a membrane environment that more closely mimics the negatively charged bacterial outer membrane.

In all samples, folded Ail migrates as a single homogenous band on SDS-PAGE and exhibits the typical shift in apparent molecular weight, relative to unfolded protein, that is associated with the heat modifiability property of transmembrane β-barrels [39]. Unfolded Ail migrates just above 21 kDa, while Ail preparations in DMPC or DePC migrate near 14 kDa, and preparations in DMPC/DMPG nanodiscs migrate between 14 and 21 kDa. This difference may be due to the residual association of Ail with the negatively charged phospholipid DMPG or with the MSP required for nanodisc formation. Although Ail and MSP have similar molecular weights and migrate as a single band on SDS-PAGE, the corresponding Western blots probed with either anti-Ail-EL2 or anti-ApoA1 antibodies show that Ail nanodiscs do indeed contain both Ail and MSP, while empty nanodiscs lacking Ail yield only MSP signal (Fig. 1B).

Lipid nanodiscs, and their larger analogs macrodiscs, have the important advantages of being detergent-free as well as open systems [5,12]. Since both lipid bilayer leaflets are exposed to the same aqueous solution, they are better suited for functional and ligand binding assays than sealed liposomes [51]. Indeed, Western dot blots probed with anti-Ail-EL2 or anti-His antibody (Fig. 1C) show that when Ail is incorporated in nanodiscs its second extracellular loop (EL2) and its intracellular C-terminus are equally accessible to the aqueous environment, since equally strong signals are obtained with either anti-Ail-EL2 or anti-His antibody. By contrast, the signals observed for Ail in liposomes have equal but significantly attenuated intensities, suggesting the presence of two equal populations of Ail in these samples: one with the extracellular loops facing the vesicle interior and the other facing the exterior. The observation of equal attenuated signals from both ends of the protein is consistent with the formation of sealed and/or multilamellar liposomes.

Two molecules of scaffold protein are needed to form one phospholipid nanodisc [12,38]. However, the precise ratio of MSP to lipid molecules depends on the specific nature of both the MSP and the membrane protein that is embedded in the lipid bilayer. Size exclusion chromatography analysis (Fig. 1D) of Ail nanodiscs shows that preparations with an Ail/MSP/phospholipid ratio of 0.5/2/100 yield the narrowest elution profiles and, hence, have the greatest size homogeneity (Fig. 1D, red). This ratio yields Ail nanodiscs with similar homogeneity to empty nanodiscs (Fig. 1D, 0/2/100) and also supports a higher membrane protein concentration corresponding to one molecule of Ail per nanodisc (Fig. 1D, 1/2/100), which is useful for enhancing the signals in both the NMR spectra and the functional assays.

Attempts to use Ni-affinity chromatography to isolate Ail–His-containing nanodiscs from empty nanodiscs resulted in extensive aggregation (Fig. S4). This appears to be due to the interaction of residual Ni^{2+} ions with the negatively charged phosphate groups of the phospholipids, as the effect could be reversed, albeit not completely by the addition of EDTA. Therefore, since nanodiscs prepared with Ail/MSP/phospholipid ratios of 1/2/100 have a homogeneous size exclusion profile they were used directly for binding assays and NMR studies.

3.2. Ail adopts an eight-stranded β-barrel conformation in detergent micelles

The crystal structure of Ail has been determined in tetraethylene glycol monooctyl ether (C_8E_4) at a high resolution [28]. In this structure, several residues in the functionally important extracellular loops EL2 and EL3 were disordered and incompletely resolved, reflecting the presence of backbone flexibility and precluding crystallographic structure–activity studies of Ail–ligand interactions. To characterize the conformation and dynamics of Ail we performed NMR studies designed to obtain backbone resonance assignments, distance restraints and dynamics parameters.

Extensive screening for detergents suitable for high resolution NMR spectroscopy of Ail identified DePC as the top candidate (Fig. 2A, S5 [40]), as previously reported for two other outer membrane proteins, OmpX and OmpW [52,53]. Ail in 170 mM DePC, at 45 °C, yields a well-resolved

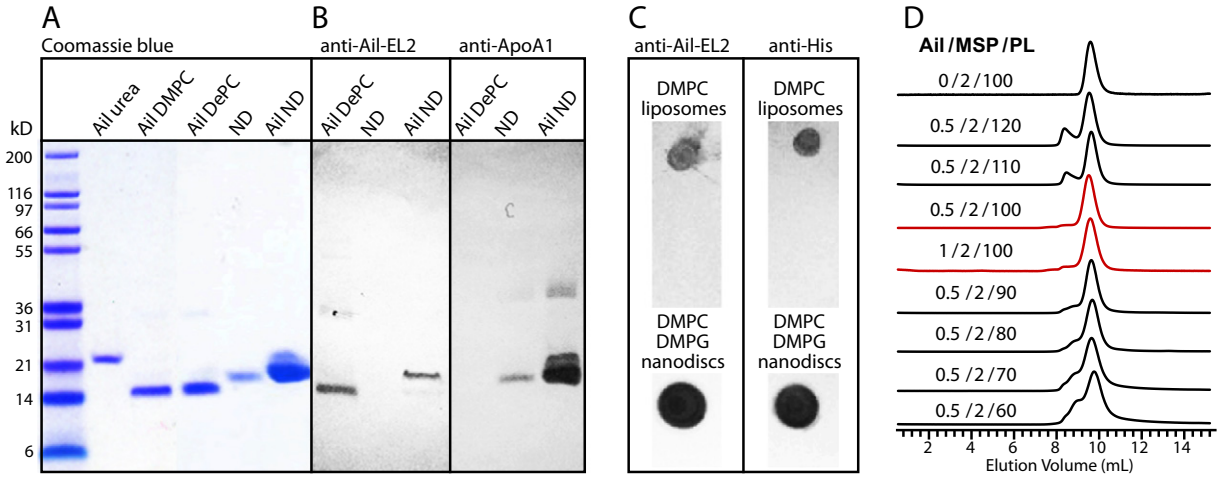

Fig. 1. Characterization of Ail in detergent, liposomes and nanodiscs. (A, B) SDS PAGE of Ail unfolded in urea (Ail urea), or folded in DMPC liposomes (Ail DMPC), 4 mM DePC (Ail DePC) and nanodiscs (Ail ND). Empty nanodiscs (ND) are shown for comparison. The gels were visualized with Coomassie blue stain (A), or by Western blot (B) probed with Ail-EL2 antibody or ApoA1 antibody. (C) Western dot blots probed with anti-Ail-EL2 or anti-His antibody to detect EL2 or the C-terminus of Ail in liposome or nanodisc preparations. (D) Size exclusion chromatography of Ail nanodiscs with varying molar ratios of Ail to MSP to phospholipid (Ail/MSP/PL). Ratios of 0.5/2/100 or 1/2/100 yield the most homogenous nanodiscs (red) with the least amount aggregation.

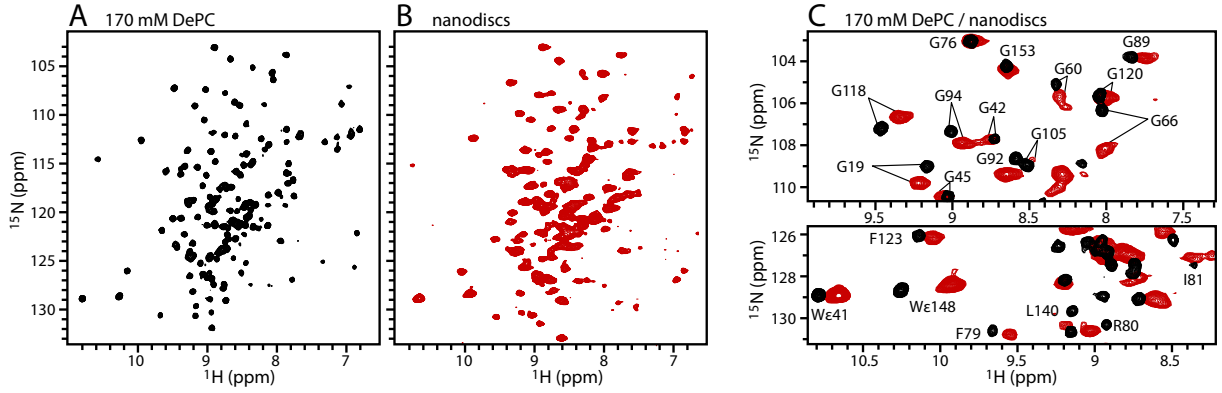

Fig. 2. NMR $^{1}H/^{15}N$ correlation spectra of Ail in DePC and nanodiscs. (A) Ail in 170 mM DePC. (B) Ail in DMPC/DMPG nanodiscs prepared with MSP1D1Δh5 at Ail/MSP/lipid molar ratio of 1/2/100 and DMPC/DMPG molar ratio of 3/1. (C) Overlay of $^{1}H/^{15}N$ spectra of Ail in 170 mM DePC (black) and nanodiscs (red).

$^{1}H/^{15}N$ correlation spectrum with narrow, homogenous resonance linewidths and large chemical shift dispersions, consistent with an overall ordered fold and relatively uniform backbone dynamics across the entire protein sequence. Assignments of the backbone (CA, CB, N, and HN) resonances were obtained for all Ail amino acids, with the exception of three residues in IL1 (Ile36, Phe37, Asn38) and two residues in IL2 (Glu83, Tyr84).

The experimental NMR data, including the values of the assigned chemical shifts, amide ^{1}H NOE connectivities and amide ^{1}H exchange profile, reflect the formation of eight anti-parallel β-strands that fold as a β-barrel (Fig. 3). The locations of the β-strands and connecting loops determined by NMR match those observed in the crystal structure of Ail and coincide with the transmembrane core of the barrel being defined by the presence of two bands of aromatic residues, each delimiting the intra- and extracellular membrane–water interfaces (Fig. 3A, B).

The $^{1}H/^{2}H$ exchange data, obtained by acquiring $^{1}H/^{15}N$ NMR spectra after equilibrating the sample in $^{2}H_2O$ for at least 4 h, show that the protein fold is stabilized by a strong network of backbone amide hydrogen bonds that resist exchange with water (Fig. 3C). Stronger hydrogen bonds are observed for residues that form a hydrophobic band around the β-barrel, consistent with their likely location in the detergent micelle interior. By contrast, weak and readily exchangeable hydrogen bonds are observed for residues located in regions outside of the hydrophobic band that are in contact with the surrounding water.

A network of long-range NOEs, detected between backbone amide HN atoms more than 4 residues apart in the protein sequence, provides diagnostic evidence of β-barrel formation (Fig. 3C). NOE contacts are observed between all eight β-strands (β1–β2, β2–β3, β3–β4, β4–β5, β5–β6, β6–β7, β7–β8), including key contacts between β1–β8 that define the barrel closure (Fig. S6). Furthermore, NOEs are observed both in the transmembrane core of the barrel and in the extracellular region.

The measured heteronuclear $^{1}H/^{15}N$ NOEs reflect the presence of relatively uniform backbone dynamics throughout the β-barrel core of

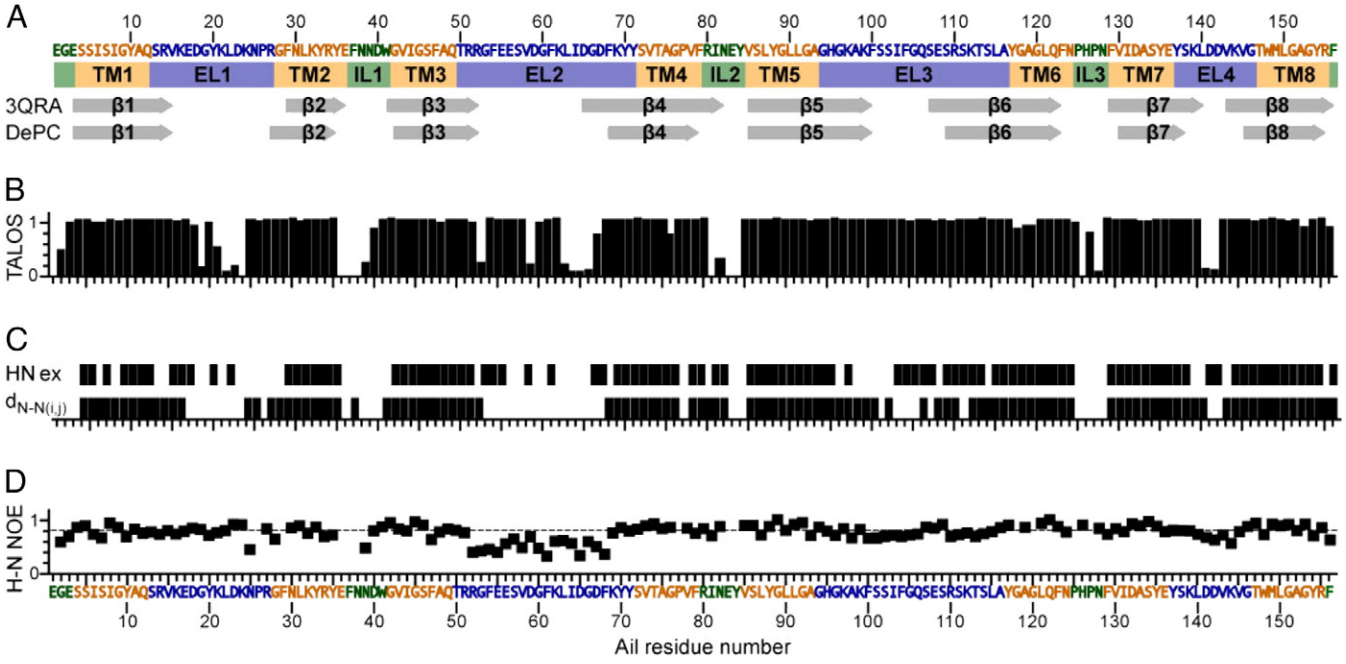

Fig. 3. Secondary structure and backbone dynamics of Ail in 170 mM DePC versus residue number. (A) Topology of Ail; colors designate the eight transmembrane regions (TM1-8; gold), three intracellular loops (IL1-4; green) and four extracellular loops (EL1-4; blue) of Ail. The eight β-strands observed in the crystal structure (3QRA) or derived from the experimental NMR data (DePC) are shown. (B) TALOS analysis of the assigned CA, CB, N, and HN chemical shifts. The height of the bars reflects β-strand probability extracted from the TALOS neural network phi/psi distribution prediction. (C) Experimental amide $^{1}H/^{2}H$ exchange data (HN ex) showing residues with amide $^{1}H/^{15}N$ NMR signals that persist for at least 4 h in $^{2}H_2O$, and experimental amide ^{1}HN-^{1}HN NOE data ($d_{N-N(i-j)}$), showing long-range NOE connectivities at least four residues apart. (D) Experimental heteronuclear $^{1}H/^{15}N$ NOE data. Residues in EL2 have values below 0.8 (dashed horizontal line).

Ail (Fig. 3D). Most residues, including those in the N- and C-termini, exhibit very similar, positive $^{1}H/^{15}N$ NOE values (≥ 0.8), indicative of a rigid backbone conformation. However, lower values are observed for residues in the extracellular loops, indicating the presence of additional restricted motions, with modest decreases observed in EL1, EL3 and EL4 and significantly lower values (between 0.8 and 0.5) observed for EL2. This loop flexibility is consistent with the lack of electron density observed in the crystal structure for residues in EL2 and EL3.

The combined NMR data show that Ail is folded correctly in DePC with a conformation that is very similar to the crystal structure and backbone dynamics that are consistent with flexibility in the functionally important extracellular loops.

3.3. Micellar detergent concentrations disrupt the ligand binding activity of Ail

We next tested the ability of Ail to bind its ligands heparin and fibronectin. To test the fibronectin binding activity we performed pull-down assays on Ni-NTA resin. We found that plasma fibronectin spontaneously binds Ni-NTA (Fig. 4A). Incubation of fibronectin with Ni-NTA agarose, followed by separation of the supernatant from the resin and elution with SDS-PAGE sample buffer, shows that fibronectin is absent from the unbound and wash fractions (Fig. 4A, lanes U, W), but present in the bound fraction that elutes with SDS (Fig. 4A, lane E). By contrast, the same experiment performed with refolded, non His-tagged Ail in DePC shows that Ail does not bind Ni-NTA (Fig. 4B). In this case, Ail was found completely in the unbound fraction and absent from the bound elution.

In 4 mM DePC, below the 11 mM critical micelle concentration (CMC), Ail displays the higher SDS-PAGE mobility (near 14 kDa) characteristic of the folded state (Fig. 4B). Furthermore, when Ail and fibronectin were first mixed together and then added to Ni-NTA in 4 mM DePC, both proteins co-eluted in SDS and neither could be detected in the unbound fraction (Fig. 4C), indicating that this low concentration of detergent supports the interaction of Ail with fibronectin. Similarly, Ail in 4 mM DePC is also capable of binding heparin-coated resin (Fig. 4D) consistent with previous results [28]. However, when the assay was performed at either the NMR sample conditions (170 mM DePC) or lower detergent concentrations (70 and 35 mM DePC) no interaction was detected between Ail and fibronectin (Fig. 4C): while fibronectin still bound the Ni-NTA resin, Ail did not, and was found completely in the unbound flow through.

We next examined whether 4 mM DePC could yield useful NMR spectra of Ail for parallel NMR and activity studies. However, despite the visually clear appearance of the sample, the $^{1}H/^{15}N$ NMR spectrum of Ail in 4 mM DePC is invisible (Fig. 5A, bottom), indicating that the protein is motionally restricted with correlation times slower than the solution NMR time scale. This result is consistent with the vast majority of membrane protein NMR studies where detergent concentrations well above the CMC are needed to ensure the presence of a single protein molecule per micelle [52,54,55].

The NMR spectra of Ail in different concentrations of DePC show that the spectral quality is also rather degraded at both 70 mM and 35 mM DePC (Fig. 5A, B). Overall, reducing the DePC concentration from 170 to 70 mM causes a 30% decrease of the NMR signal intensity, and further reduction to 35 mM decreases the signal by an additional 30%. The observed signal decrease is not uniform across all peaks. For example, the signal from Phe68, in extracellular loop EL2, is completely obliterated at 35 mM DePC, while the signal from Asn128, in intracellular loop IL3, has much lower intensity but is still visible at 35 mM DePC.

Increasing the concentration of DePC from 35 to 170 mM also induces visible changes in the ^{1}H and ^{15}N chemical shifts of the spectrum (Fig. 5C). This effect appears to be most significant for peaks arising from sites in the extracellular loops of the protein, such as Gly60 and Gly66 in EL2, and Ile103 and Gly105 in EL3. Since the loops are not expected to interact with the micelle, this effect could reflect either progressive protein dilution in increasing amounts of detergent or the association of monomeric detergent with the water-exposed loops. Thus we conclude that while Ail is folded and active in 4 mM DePC, the higher concentrations of DePC required for NMR spectroscopy, are not compatible with protein activity, precluding structure and activity studies in DePC micelles.

Previously, we reported that DHPC (1,2-dihexyl-sn-glycero-3-phosphocholine) also yields good NMR spectra of Ail [40], and therefore, we tested this detergent for its ability to support protein binding activity. Disruption of the fibronectin binding activity was observed with 20 mM DHPC (Fig. S2C), well below the 240 mM concentration that yields useful spectra of Ail (Fig. S5) [40] and the 300 mM concentration that was used for structure determination of OmpX [56]. In addition, since 1 mM DDM (n-dodecyl-β-D-maltopyranoside) was used for previous refolding and activity studies of Ail [28], we tested this detergent for its ability to yield high-resolution NMR spectra. However, we found that a 20 mM concentration of DDM both disrupts fibronectin binding (Fig. S2D) and yields very low quality NMR spectra (Fig. S7E).

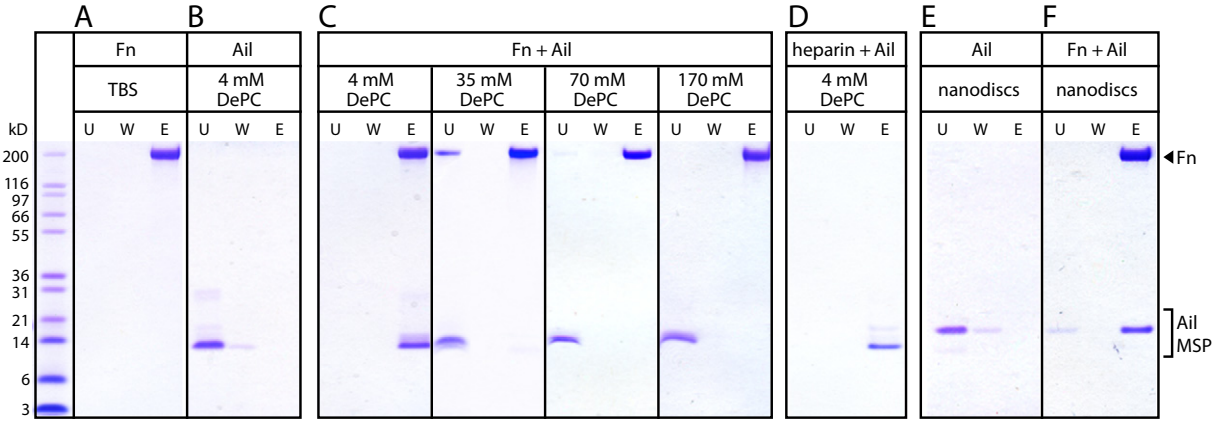

Fig. 4. Fibronectin (Fn) and heparin binding activity of Ail detected by pull-down assays. Ail alone, Fn alone, or Fn plus Ail was mixed with heparin or Ni-NTA agarose beads. None of the proteins contain His tags. After overnight incubation at 37 °C, the unbound fraction (lane U) was separated by centrifugation, the beads were washed with TBS (lane W) and centrifuge separated. After a second wash and centrifugation step any bound protein was eluted with 100 mM SDS (lane E). All fractions were analyzed by SDS PAGE and visualized with Coomassie blue. (A) Fn binds Ni-NTA. (B) Ail does not bind Ni-NTA. (C) Fn binds Ail in 4 mM DePC; the proteins elute together in the Ni-NTA-bound fraction (lane E). Fn does not bind Ail in either 35, 70 or 170 mM DePC; the proteins elute separately (Ail in lane U; Fn in lane E). (D) Ail in 4 mM DePC binds heparin-coated beads and is found in the elution fraction (lane E). (E) Ail in nanodiscs does not bind Ni-NTA. (F) Fn binds Ail in nanodiscs; the proteins elute together in the Ni-NTA-bound fraction (lane E).

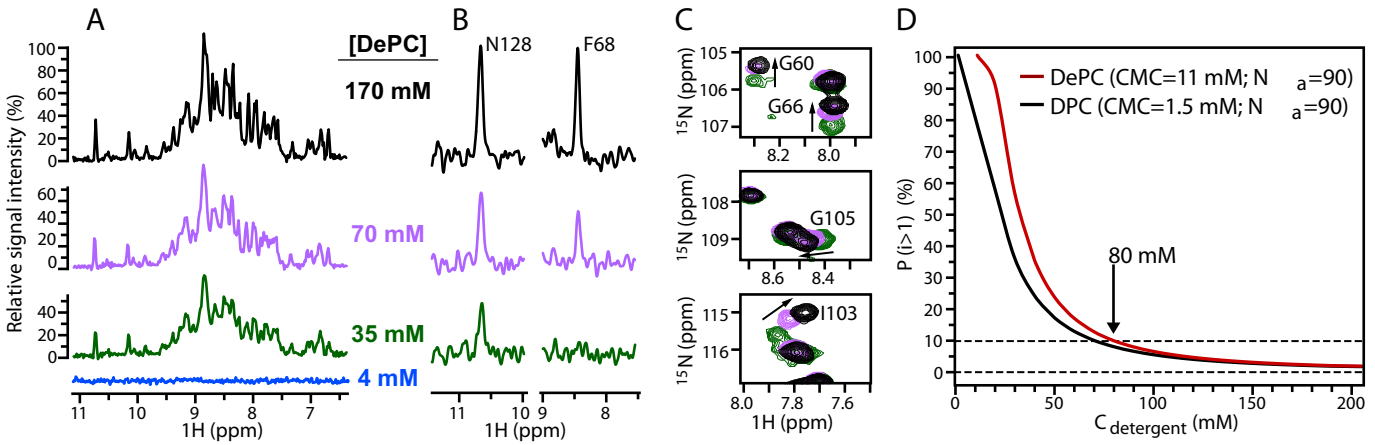

Fig. 5. Effect of detergent concentration on the NMR spectra of Ail. (A, B) One-dimensional ^{1}H NMR spectra (A) and spectral slices from two-dimensional $^{1}H/^{15}N$ correlation spectra (B) for Ail in 170 mM (top), 70 mM (middle) and 35 mM (bottom) DePC. (C) Two-dimensional $^{1}H/^{15}N$ correlation spectra of Ail in 170 mM (black), 70 mM (pink) and 35 mM (green) DePC. (D) Probability of finding more than one protein per micelle P(i > 1) as a function of detergent concentration ($C_{detergent}$), calculated from Eq. 4, for 0.4 mM protein, with CMC and N_a values [52] of DePC (red) and DPC (black).

3.4. Micellar detergent concentrations are needed for high resolution NMR spectroscopy of Ail

Detergent concentration has long been known to influence the quality of NMR spectra. High detergent concentrations well above the CMC are needed to ensure the presence of no more than one protein or protein complex per micelle, which is essential for maintaining sufficiently rapid correlation times for solution NMR [52,54]. This effect may be understood in terms of the probability distribution of protein molecules in micelles, with the probability P(i) of finding i proteins per micelle given by:

$$P(i) = n^{i}\left(\frac{e^{-n}}{i!}\right) \quad (1)$$

where n, the total number of proteins per micelle, depends on the protein concentration ($C_{protein}$) and the micelle concentration ($C_{micelle}$) as:

$$n = \frac{C_{protein}}{C_{micelle}} \quad (2)$$

and $C_{micelle}$ depends on the detergent's concentration ($C_{detergent}$), aggregation number (N_a) and CMC as:

$$C_{micelle} = \frac{C_{detergent} - CMC}{N_a}. \quad (3)$$

The probability P(i > 1) of finding more than one protein per micelle is derived from Eqs. 1–3 and given by:

$$\begin{aligned} P(i>1) &= 1 - P(i=0) - P(i=1) \\ &= 1 - e^{-n} - ne^{-n} \end{aligned}. \quad (4)$$

For solution NMR studies, P(i > 1) should be minimized as much as possible. The plot in Fig. 5D shows that, for the sample conditions used in this study (0.4 mM protein in DePC), P(i > 1) increases sharply above 10% at DePC concentrations lower than 80 mM. By contrast, above 80 mM DePC, P(i > 1) decreases slowly down to near 0% at 200 mM. Above such high levels of detergents, the NMR spectral quality has been shown to decrease [52] as the deleterious effects of sample viscosity begin to counter the benefits of protein dispersion.

Probability curves calculated for detergents with a lower CMC, such as DPC (n-dodecyl-phosphocholine), display the same effect, albeit with lower detergent concentration limits (Fig. 5D, black). Such probability analysis is consistent with our observation of a sharp NMR signal intensity reduction below 70 mM DePC and with previous results for the effects of detergent concentration on the NMR spectra of membrane proteins [52,54].

3.5. Phospholipid nanodiscs yield high resolution NMR spectra of Ail and support ligand binding activity

Y. pestis Ail incorporated in MSP1D1Δh5 nanodiscs yields excellent $^{1}H/^{15}N$ correlation NMR spectra with many well-resolved, well-dispersed peaks of homogeneous intensity (Fig. 2B). Although the ^{1}H and ^{15}N resonance lines are broader compared to the spectra of Ail in DePC, there are many peaks with similar chemical shifts (Fig. 2C, S3C), indicating that the protein adopts a similar conformation in micelles and nanodiscs. Many peaks, including several from Gly, Trp and Phe residues, appear at nearly identical positions and can be tentatively assigned to specific sites by comparison with the assigned spectrum of Ail in DePC. At first inspection, the similarities appear more significant for peaks from sites in the transmembrane β-barrel (e.g. G42, G45, G76, G89, G120, G151, G153), while peaks from water-exposed residues display larger differences (e.g. T50, G66, F68, N128, L140, R155). Independent resonance assignments of the Ail nanodisc spectrum (in progress) will be needed to confirm this observation. However, it is notable that for OmpX and OmpA, the largest effects of detergent were observed in the structure and dynamics of the water-exposed loops [18,23].

Importantly, when the Ni-NTA fibronectin binding assay is performed with Ail in nanodiscs instead of detergent micelles, fibronectin binding activity is observed. Ail-containing nanodiscs do not bind Ni-NTA resin in the absence of fibronectin and are recovered in the unbound supernatant fraction (Fig. 4E). However, when Ail nanodiscs are first mixed with fibronectin and then added to the resin, both proteins co-elute in SDS with negligible amount of nanodiscs detected in the unbound fraction (Fig. 4F). Thus, we conclude that the fibronectin binding activity of Ail, which was disrupted in detergent micelles, is restored when the protein is incorporated in a detergent-free phospholipid bilayer.

To characterize the fibronectin-binding activity of Ail in assays amenable to quantitative, high-throughput analysis, we tested its ability to bind fibronectin-coated surfaces in ELISAs. Consistent with the pull-down assays, Ail in 4 mM DePC exhibits concentration-dependent binding to fibronectin-coated plates (Fig. 6A, black), while the 170 mM concentration of detergent that is optimal for NMR induces complete disruption of the protein–protein interaction (Fig. 6A, blue). Once again, incorporation of Ail in nanodiscs and removal of detergent restore

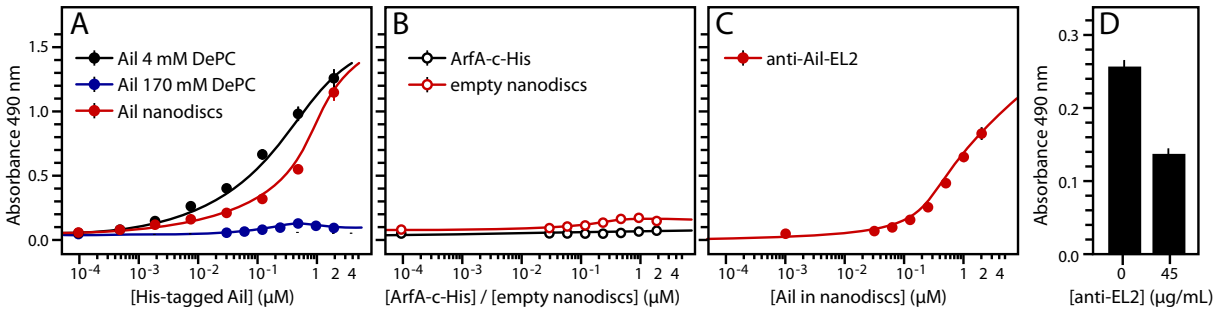

Fig. 6. Fibronectin binding activity of Ail detected by enzyme linked immunosorbent assay (ELISA). (A) Purified refolded Ail–His was added at increasing concentrations to fibronectin-coated plates and incubated overnight. Binding was detected by ELISA using a mouse anti-His antibody. Ail–His in 4 mM DePC (black) and Ail–His in nanodiscs (red) bind fibronectin. Ail–His in 170 mM DePC (blue) does not bind fibronectin. (B) Negative controls. Empty nanodiscs lacking Ail–His (red), or the unrelated His-tagged soluble protein ArfA-c (black), were added to fibronectin-coated plates and binding was probed with anti-His or anti-ApoA1 antibodies. No binding is detected. (C) Plates were coated with increasing concentrations of Ail nanodiscs and Ail was detected with anti-Ail-EL2 antibody. (D) Purified refolded Ail–His in nanodiscs (at 0.06 μM Ail concentration), was incubated with 0 or 45 μg/mL anti-EL2 antibody, then added to fibronectin-coated plates and detected by ELISA using mouse anti-His antibody. Each point in each data set represents the average of three experiments.

the fibronectin binding activity of the protein (Fig. 6A, red). Assays performed with empty nanodiscs, or with an unrelated protein (ArfA-c) from *M. tuberculosis*, yield no ELISA signal (Fig. 6B), and thus confirm that any fibronectin binding signal is due to Ail in these experiments.

We further examined the usefulness of Ail nanodiscs as an ELISA coating substrate. The data show that increasing concentrations of Ail nanodiscs can be effectively immobilized on 96-well plates for detection by anti-Ail-EL2 antibody (Fig. 6C), thereby providing an approach to screen for compounds that interfere with ligand binding.

Finally, to examine the role of Ail's extracellular loops in mediating the interaction of the protein with fibronectin, we performed competition ELISAs in the presence of anti-Ail-EL2 antibody. Incubation of Ail with anti-Ail-EL2 before addition to fibronectin-coated plates substantially diminishes the Ail-fibronectin interaction and yields a significant decrease in ELISA signal (Fig. 6D), demonstrating that the extracellular loops of Ail are involved in mediating its interaction with fibronectin. The antibody was raised specifically to bind EL2 and, therefore, is expected to block ligand binding to this region of Ail. However, its molecular size may be sufficiently large to interfere with the interactions mediated by any or all of four extracellular loops. Therefore, the fibronectin binding activity cannot be exclusively ascribed to EL2 based on this assay. Indeed, residues in EL1 and EL3 have also been identified for the adhesion activity of *Y. pestis* Ail [36]. Additional experiments designed to probe specific areas of Ail will be needed to describe the Ail–fibronectin interaction more precisely.

4. Conclusions

Our results show that the structure and ligand binding activities of *Y. pestis* Ail can be reconstituted in phospholipid bilayer nanodiscs enabling NMR and activity studies to be performed in identical samples. The NMR data show that Ail adopts its correct eight-stranded β-barrel conformation in DePC micelles and that its overall structure appears to be similar in nanodiscs. However, while Ail in nanodiscs is capable of binding its human ligand fibronectin, the high detergent concentrations required for NMR studies in micelles disrupt the fibronectin-binding activity. Since the ELISA data further show that the extracellular loops of Ail are involved in mediating its interaction with fibronectin, we conclude that the disruption of fibronectin binding in detergent micelles is likely caused by the interaction of monomeric detergent molecules with key water-exposed sites on Ail and/or fibronectin.

Detergents can have deleterious effects on membrane protein structure and function [2]. Monomeric detergent is always present in equilibrium with the micellar phase and is often observed bound to crystallized membrane proteins, including Ail [28]. Experimental and computational studies indicate that the extracellular loops of outer membrane β-barrels are more susceptible to the surrounding environment than their transmembrane segments. Compared to lipid bilayer nanodiscs, the largest effects of detergent micelles on the structure and dynamics of *E. coli* OmpX and OmpA are observed for the extramembrane loops [18,23]. Furthermore, micelles and bilayers differ significantly with respect to their lateral pressure profiles, water accessibility and order, all factors that could contribute to altered protein binding properties. For example, molecular dynamics simulations of *Neisseria* Opa_{60}, another eight-stranded β-barrel whose NMR structure was recently determined in DPC micelles, indicate that the lipid bilayer environment influences the compactness and dynamics of the protein's extracellular loops [24]. The presence of detergent could also induce the exposure of adventitious binding sites on the Ail β-barrel and yield apparently higher ligand binding affinities.

Nanodiscs are detergent-free and provide a phospholipid bilayer environment that recapitulates the key anisotropic physical and chemical properties of biological membranes [11,12]. The use of such open lipid bilayer samples facilitates structure–activity studies where the addition of small molecule or protein ligands is detected by direct spectroscopic and structural comparisons. While the increased size of such complexes may be prohibitive for solution NMR spectroscopy, solid-state NMR has no size limitations and can be used with proteins in larger sized macrodiscs [5] or surface-supported planar bilayers [57] for analogous structure–activity studies of membrane proteins in detergent-free native-like samples.

Acknowledgements

We thank Eva Engvall for valuable advice on ELISA development and optimization. This research was supported by a grant from the National Institutes of Health (GM100265). The NMR studies utilized the Cancer Center NMR Facility at Sanford-Burnham Medical Research Institute, supported by the NIH (P30 CA030199).

Appendix A. Supplementary data

Supplementary data to this article can be found online at http://dx.doi.org/10.1016/j.bbamem.2014.11.021.

References

[1] C.B. Anfinsen, Principles that govern the folding of protein chains, Science 181 (1973) 223–230.
[2] H.X. Zhou, T.A. Cross, Influences of membrane mimetic environments on membrane protein structures, Annu. Rev. Biophys. 42 (2013) 361–392.
[3] S.B. Shuker, P.J. Hajduk, R.P. Meadows, S.W. Fesik, Discovering high-affinity ligands for proteins: SAR by NMR, Science 274 (1996) 1531–1534.
[4] A. McDermott, Structure and dynamics of membrane proteins by magic angle spinning solid-state NMR, Annu. Rev. Biophys. 38 (2009) 385–403.
[5] S.H. Park, S. Berkamp, G.A. Cook, M.K. Chan, H. Viadiu, S.J. Opella, Nanodiscs versus macrodiscs for NMR of membrane proteins, Biochemistry 50 (2011) 8983–8985.

[6] W.T. Franks, A.H. Linden, B. Kunert, B.J. van Rossum, H. Oschkinat, Solid-state magic-angle spinning NMR of membrane proteins and protein–ligand interactions, Eur. J. Cell Biol. 91 (2012) 340–348.
[7] S.H. Park, B.B. Das, F. Casagrande, Y. Tian, H.J. Nothnagel, M. Chu, H. Kiefer, K. Maier, A. De Angelis, F.M. Marassi, S.J. Opella, Structure of the chemokine receptor CXCR1 in phospholipid bilayers, Nature 491 (2012) 779–783.
[8] N. Das, D.T. Murray, T.A. Cross, Lipid bilayer preparations of membrane proteins for oriented and magic-angle spinning solid-state NMR samples, Nat. Protoc. 8 (2013) 2256–2270.
[9] S. Wang, R.A. Munro, L. Shi, I. Kawamura, T. Okitsu, A. Wada, S.Y. Kim, K.H. Jung, L.S. Brown, V. Ladizhansky, Solid-state NMR spectroscopy structure determination of a lipid-embedded heptahelical membrane protein, Nat. Methods 10 (2013) 1007–1012.
[10] K. Yamamoto, M.A. Caporini, S. Im, L. Waskell, A. Ramamoorthy, Shortening spin-lattice relaxation using a copper-chelated lipid at low-temperatures — a magic angle spinning solid-state NMR study on a membrane-bound protein, J. Magn. Reson. 237 (2013) 175–181.
[11] A. Nath, W.M. Atkins, S.G. Sligar, Applications of phospholipid bilayer nanodiscs in the study of membranes and membrane proteins, Biochemistry 46 (2007) 2059–2069.
[12] T.K. Ritchie, Y.V. Grinkova, T.H. Bayburt, I.G. Denisov, J.K. Zolnerciks, W.M. Atkins, S.G. Sligar, Chapter 11 — Reconstitution of membrane proteins in phospholipid bilayer nanodiscs, Methods Enzymol. 464 (2009) 211–231.
[13] J.M. Gluck, M. Wittlich, S. Feuerstein, S. Hoffmann, D. Willbold, B.W. Koenig, Integral membrane proteins in nanodiscs can be studied by solution NMR spectroscopy, J. Am. Chem. Soc. 131 (2009) 12060–12061.
[14] T. Raschle, S. Hiller, T.Y. Yu, A.J. Rice, T. Walz, G. Wagner, Structural and functional characterization of the integral membrane protein VDAC-1 in lipid bilayer nanodiscs, J. Am. Chem. Soc. 131 (2009) 17777–17779.
[15] Z.O. Shenkarev, E.N. Lyukmanova, O.I. Solozhenkin, I.E. Gagnidze, O.V. Nekrasova, V.V. Chupin, A.A. Tagaev, Z.A. Yakimenko, T.V. Ovchinnikova, M.P. Kirpichnikov, A.S. Arseniev, Lipid–protein nanodiscs: possible application in high-resolution NMR investigations of membrane proteins and membrane-active peptides, Biochemistry (Mosc) 74 (2009) 756–765.
[16] Z.O. Shenkarev, E.N. Lyukmanova, A.S. Paramonov, L.N. Shingarova, V.V. Chupin, M.P. Kirpichnikov, M.J. Blommers, A.S. Arseniev, Lipid–protein nanodiscs as reference medium in detergent screening for high-resolution NMR studies of integral membrane proteins, J. Am. Chem. Soc. 132 (2010) 5628–5629.
[17] M. Etzkorn, T. Raschle, F. Hagn, V. Gelev, A.J. Rice, T. Walz, G. Wagner, Cell-free expressed bacteriorhodopsin in different soluble membrane mimetics: biophysical properties and NMR accessibility, Structure 21 (2013) 394–401.
[18] F. Hagn, M. Etzkorn, T. Raschle, G. Wagner, Optimized phospholipid bilayer nanodiscs facilitate high-resolution structure determination of membrane proteins, J. Am. Chem. Soc. 135 (2013) 1919–1925.
[19] K. Mors, C. Roos, F. Scholz, J. Wachtveitl, V. Dotsch, F. Bernhard, C. Glaubitz, Modified lipid and protein dynamics in nanodiscs, Biochim. Biophys. Acta 1828 (2013) 1222–1229.
[20] Z.O. Shenkarev, E.N. Lyukmanova, I.O. Butenko, L.E. Petrovskaya, A.S. Paramonov, M.A. Shulepko, O.V. Nekrasova, M.P. Kirpichnikov, A.S. Arseniev, Lipid–protein nanodiscs promote in vitro folding of transmembrane domains of multi-helical and multimeric membrane proteins, Biochim. Biophys. Acta 1828 (2013) 776–784.
[21] C. Tzitzilonis, C. Eichmann, I. Maslennikov, S. Choe, R. Riek, Detergent/nanodisc screening for high-resolution NMR studies of an integral membrane protein containing a cytoplasmic domain, PLoS ONE 8 (2013) e54378.
[22] S. Bibow, M.G. Carneiro, T.M. Sabo, C. Schwiegk, S. Becker, R. Riek, D. Lee, Measuring membrane protein bond orientations in nanodiscs via residual dipolar couplings, Protein Sci. 23 (2014) 851–856.
[23] L. Susac, R. Horst, K. Wuthrich, Solution-NMR characterization of outer-membrane protein A from *E. coli* in lipid bilayer nanodiscs and detergent micelles, Chembiochem 15 (2014) 995–1000.
[24] D.A. Fox, P. Larsson, R.H. Lo, B.M. Kroncke, P.M. Kasson, L. Columbus, The structure of the Neisserial outer membrane protein Opa: loop flexibility essential to receptor recognition and bacterial engulfment, J. Am. Chem. Soc. 136 (2014) 9938–9946.
[25] R.D. Perry, J.D. Fetherston, *Yersinia pestis*—etiologic agent of plague, Clin. Microbiol. Rev. 10 (1997) 35–66.
[26] G.R. Cornelis, Molecular and cell biology aspects of plague, Proc. Natl. Acad. Sci. U. S. A. 97 (2000) 8778–8783.
[27] R.R. Brubaker, The recent emergence of plague: a process of felonious evolution, Microb. Ecol. 47 (2004) 293–299.
[28] S. Yamashita, P. Lukacik, T.J. Barnard, N. Noinaj, S. Felek, T.M. Tsang, E.S. Krukonis, B.J. Hinnebusch, S.K. Buchanan, Structural insights into Ail-mediated adhesion in *Yersinia pestis*, Structure 19 (2011) 1672–1682.
[29] A.M. Kolodziejek, D.J. Sinclair, K.S. Seo, D.R. Schnider, C.F. Deobald, H.N. Rohde, A.K. Viall, S.S. Minnich, C.J. Hovde, S.A. Minnich, G.A. Bohach, Phenotypic characterization of OmpX, an Ail homologue of *Yersinia pestis* KIM, Microbiology 153 (2007) 2941–2951.
[30] S. Felek, E.S. Krukonis, The *Yersinia pestis* Ail protein mediates binding and Yop delivery to host cells required for plague virulence, Infect. Immun. 77 (2009) 825–836.
[31] S.S. Bartra, K.L. Styer, D.M. O'Bryant, M.L. Nilles, B.J. Hinnebusch, A. Aballay, G.V. Plano, Resistance of *Yersinia pestis* to complement-dependent killing is mediated by the Ail outer membrane protein, Infect. Immun. 76 (2008) 612–622.
[32] S. Felek, T.M. Tsang, E.S. Krukonis, Three *Yersinia pestis* adhesins facilitate Yop delivery to eukaryotic cells and contribute to plague virulence, Infect. Immun. 78 (2010) 4134–4150.
[33] T.M. Tsang, S. Felek, E.S. Krukonis, Ail binding to fibronectin facilitates *Yersinia pestis* binding to host cells and Yop delivery, Infect. Immun. 78 (2010) 3358–3368.
[34] T.M. Tsang, D.S. Annis, M. Kronshage, J.T. Fenno, L.D. Usselman, D.F. Mosher, E.S. Krukonis, Ail protein binds ninth type III fibronectin repeat (9FNIII) within central 120-kDa region of fibronectin to facilitate cell binding by *Yersinia pestis*, J. Biol. Chem. 287 (2012) 16759–16767.
[35] V.L. Miller, K.B. Beer, G. Heusipp, B.M. Young, M.R. Wachtel, Identification of regions of Ail required for the invasion and serum resistance phenotypes, Mol. Microbiol. 41 (2001) 1053–1062.
[36] T.M. Tsang, J.S. Wiese, S. Felek, M. Kronshage, E.S. Krukonis, Ail proteins of *Yersinia pestis* and *Y. pseudotuberculosis* have different cell binding and invasion activities, PLoS ONE 8 (2013) e83621.
[37] J. Sambrook, E.F. Fritsch, T. Maniatis, Molecular Cloning: A Laboratory Manual, 2nd ed. Cold Spring Harbor Laboratory, Cold Spring Harbor, N.Y., 1989
[38] I.G. Denisov, Y.V. Grinkova, A.A. Lazarides, S.G. Sligar, Directed self-assembly of monodisperse phospholipid bilayer nanodiscs with controlled size, J. Am. Chem. Soc. 126 (2004) 3477–3487.
[39] L.K. Tamm, H. Hong, B. Liang, Folding and assembly of beta-barrel membrane proteins, Biochim. Biophys. Acta 1666 (2004) 250–263.
[40] L.A. Plesniak, R. Mahalakshmi, C. Rypien, Y. Yang, J. Racic, F.M. Marassi, Expression, refolding, and initial structural characterization of the *Y. pestis* Ail outer membrane protein in lipids, Biochim. Biophys. Acta 1808 (2011) 482–489.
[41] K. Pervushin, R. Riek, G. Wider, K. Wuthrich, Attenuated T2 relaxation by mutual cancellation of dipole–dipole coupling and chemical shift anisotropy indicates an avenue to NMR structures of very large biological macromolecules in solution, Proc. Natl. Acad. Sci. U. S. A. 94 (1997) 12366–12371.
[42] M. Salzmann, K. Pervushin, G. Wider, H. Senn, K. Wuthrich, TROSY in triple-resonance experiments: new perspectives for sequential NMR assignment of large proteins, Proc. Natl. Acad. Sci. U. S. A. 95 (1998) 13585–13590.
[43] S. Grzesiek, A. Bax, Improved 3D triple-resonance NMR techniques applied to a 31 kDa protein, J. Magn. Reson. 96 (1992) 432–440.
[44] M. Wittekind, L. Mueller, HNCACB, a high-sensitivity 3D NMR experiment to correlate amide-proton and nitrogen resonances with the alpha- and beta-carbon resonances in proteins, J. Magn. Reson. Ser. B 101 (1993) 201–205.
[45] A. Bax, S. Grzesiek, Methodological advances in protein NMR, Acc. Chem. Res. 26 (1993) 131–138.
[46] N.A. Farrow, O. Zhang, J.D. Forman-Kay, L.E. Kay, A heteronuclear correlation experiment for simultaneous determination of ^{15}N longitudinal decay and chemical exchange rates of systems in slow equilibrium, J. Biomol. NMR 4 (1994) 727–734.
[47] F. Delaglio, S. Grzesiek, G.W. Vuister, G. Zhu, J. Pfeifer, A. Bax, NMRPipe: a multidimensional spectral processing system based on UNIX pipes, J. Biomol. NMR 6 (1995) 277–293.
[48] B.A. Johnson, R.A. Blevins, NMR View: a computer program for the visualization and analysis of NMR data, J. Biomol. NMR 4 (1994) 603–614.
[49] J. Cavanagh, W.J. Fairbrother, A.G. Palmer, N.J. Skelton, Protein NMR Spectroscopy: Principles and Practice, Academic Press, San Diego, 1996.
[50] Y. Shen, F. Delaglio, G. Cornilescu, A. Bax, TALOS+: a hybrid method for predicting protein backbone torsion angles from NMR chemical shifts, J. Biomol. NMR 44 (2009) 213–223.
[51] S. Inagaki, R. Ghirlando, R. Grisshammer, Biophysical characterization of membrane proteins in nanodiscs, Methods 59 (2013) 287–300.
[52] P. Stanczak, R. Horst, P. Serrano, K. Wuthrich, NMR characterization of membrane protein-detergent micelle solutions by use of microcoil equipment, J. Am. Chem. Soc. 131 (2009) 18450–18456.
[53] P. Stanczak, Q. Zhang, R. Horst, P. Serrano, K. Wuthrich, Micro-coil NMR to monitor optimization of the reconstitution conditions for the integral membrane protein OmpW in detergent micelles, J. Biomol. NMR 54 (2012) 129–133.
[54] P.A. McDonnell, S.J. Opella, Effect of detergent concentration on multidimensional solution NMR spectra of membrane proteins in micelles, J. Magn. Reson. Ser. B 102 (1993) 120–125.
[55] C.R. Sanders, K. Oxenoid, Customizing model membranes and samples for NMR spectroscopic studies of complex membrane proteins, Biochim. Biophys. Acta 1508 (2000) 129–145.
[56] C. Fernandez, K. Adeishvili, K. Wuthrich, Transverse relaxation-optimized NMR spectroscopy with the outer membrane protein OmpX in dihexanoyl phosphatidylcholine micelles, Proc. Natl. Acad. Sci. U. S. A. 98 (2001) 2358–2363.
[57] E.Y. Chekmenev, P.L. Gor'kov, T.A. Cross, A.M. Alaouie, A.I. Smirnov, Flow-through lipid nanotube arrays for structure–function studies of membrane proteins by solid-state NMR spectroscopy, Biophys. J. 91 (2006) 3076–3084.